Journal of Applied Physics

RESEARCH ARTICLE | OCTOBER 17 2024

On the physical origin of the superconducting transition in transition-edge sensors

Lourdes Fàbrega ; Agustín Camón ; Carlos Pobes ; Pavel Strichovanec

Check for updates

J. Appl. Phys. 136, 154503 (2024)
https://doi.org/10.1063/5.0225871

View Online Export Citation

Articles You May Be Interested In

Vortex dynamics in superconducting transition edge sensors

J. Appl. Phys. (February 2018)

Possible observation of the Berezinskii-Kosterlitz-Thouless transition in boron-doped diamond films

AIP Advances (November 2017)

The Berezinskii–Kosterlitz–Thouless transition in bulk MgB_2:(La,Sr)MnO_3 superconductor-ferromagnetic nanocomposites

Low Temp. Phys. (November 2019)

07 January 2025 12:38:28

AIP Publishing

Journal of Applied Physics

Special Topics Open for Submissions

Learn More

AIP Publishing

Journal of Applied Physics ARTICLE pubs.aip.org/aip/jap

On the physical origin of the superconducting transition in transition-edge sensors

Cite as: J. Appl. Phys. **136**, 154503 (2024); doi: 10.1063/5.0225871
Submitted: 27 June 2024 · Accepted: 3 October 2024 ·
Published Online: 17 October 2024

View Online Export Citation CrossMark

Lourdes Fàbrega,[1,a)] Agustín Camón,[2] Carlos Pobes,[2] and Pavel Strichovanec[2]

AFFILIATIONS

[1]Institut de Ciència de Materials de Barcelona (ICMAB-CSIC), Campus de Bellaterra, E-08193 Bellaterra, Spain
[2]Instituto de Nanociencia y Materiales de Aragón (INMA), CSIC-Universidad de Zaragoza, E-50009 Zaragoza, Spain

[a)]**Author to whom correspondence should be addressed:** lourdes@icmab.es

ABSTRACT

Transition-Edge Sensors (TESs) constitute highly sensitive particle and radiation detectors, widely used in many applications. Each of these requires optimization of TES performances and designs, including sizes and geometries. These may have implications on the superconducting transition mechanisms and, therefore, on TESs performances and stability, through the specific shape of the resistance vs temperature and current R(T,I) and the nature of noise. In this study, we investigate the dependence of the superconducting transition, characterized by R(T,I), on TES size and bias current density. Through analyses of R(T,I) in bare Mo/Au TESs with T_c tuned for this study, we observe how the weak link behavior induced by the superconducting leads weakens and disappears as TES length or driving current increase, being substituted by another dominant transition mechanism, which might be related to a Berezinskii–Kosterlitz–Thouless transition. We also observe a significant broadening of the transition's upper part, attributed to the longitudinal proximity effect induced by the pads; for the shorter devices, this effect is observed for $R > 70\%\ R_n$ and results in TES resistances considerably lower than R_n up to temperatures well above the TES transition: $R < R_n$ up to 3 K for a 8 μm-long device.

© 2024 Author(s). All article content, except where otherwise noted, is licensed under a Creative Commons Attribution-NonCommercial-NoDerivs 4.0 International (CC BY-NC-ND) license (https://creativecommons.org/licenses/by-nc-nd/4.0/). https://doi.org/10.1063/5.0225871

07 January 2025 12:38:28

I. INTRODUCTION

In a superconductor, the physical mechanisms underlying the appearance of finite resistance determine the $R(T,I)$ transition shape, i.e., the electrical resistance as a function of temperature and driving current. For Transition-Edge Sensors (TESs), this is a crucial issue, since they operate in the middle of the superconducting transition. Indeed, the $R(T,I)$ function translates directly to the logarithmic derivatives of the TES resistance with respect to temperature and current, α and β. These two parameters play key roles in TES dynamic parameters, stability, noise characteristics, and energy resolution.[1] Even more, the transition mechanisms can also generate characteristic noise that can limit the performance of a TES;[2–4] thus, knowing them is also helpful for TES optimization.

A TES is basically a thermometer, constituted by a superconducting thin film (most usually a metal/superconductor proximity bilayer) with electric contacts at both ends, which are made of a superconductor with much higher critical temperature; electrical current circulates between these contacts, whose separation is the TES length. Several models have been proposed to explain the superconducting transition of TESs. They include: the resistively shunted junction (RSJ),[5] expected to hold for TESs displaying weak link (WL) effects—caused by the longitudinal proximity effect induced by the superconducting contacts—;[6] the two fluid model;[7] phase slip lines;[8] and depairing and motion of magnetic vortex–antivortex pairs.[4,9–11]

WL effects in TESs have been unequivocally demonstrated;[3,6,12,13] they are caused by the longitudinal proximity effect induced on the superconducting film constituting the TES by the higher T_c contacts at its ends. WL effects can be observed for quite long TES lengths (~100 μm), as demonstrated in Ref. 6. The RSJ model has been proven to provide a good description of TESs displaying them; however, the origin of the transition and of excess noise in devices without evident WL effects remains debated. Moreover, the shape of the $R(T,I)$ transition in TESs is usually indirectly analyzed through the logarithmic derivatives α and β, which are typically extracted from fits to the measured complex impedance Z(ω),[14] through a procedure that has become standard. Several considerations can be made:

© Author(s) 2024

(i) α and β have been mainly analyzed in devices with absorbers.[13,15–21] Since, in principle, the one thermal block configuration most usually employed would not be enough for the electrothermal modeling of these devices,[2,22] this may introduce errors in the extracted α and β values, which might affect their experimentally determined functional dependences.

(ii) In general, the resistance of a superconductor is a highly nonlinear function of temperature and current, especially in the low resistance limit. Also, the current dependence is usually a function of the current density ratio J/J_c, where $J_c(T)$ is the critical current density, defined as the lowest current density that produces the appearance of a finite resistance in the device. Hence, the current density circulating in the TES will depend on TES width w (the in-plane TES dimension perpendicular to the current flow), while the WL effect typically observed in TESs depends on its length L,[6] which, in turn, will affect $J_c(T)$. Thus, analyzing TES parameters as a function of the aspect ratio, without taking into account whether w or L is changing together or independently, may provide a partial picture of the geometry dependences and the origin of the superconducting transition.

(iii) Most devices studied so far have banks and normal metal structures; these features, together with the absorber stems lying on the TES or tangent to it, can alter the homogeneity of the superconducting order parameter and the current distribution, thus masking the actual, intrinsic $R(T,J)$.

(iv) Finally, the dominant dissipation mechanism, i.e., the main mechanism contributing to the finite resistance of the superconductor, can change along the transition. There may be competition between different mechanisms, and the dominance of one over others will depend on T and J. Therefore, any functional dependence must be tested in several bias windows between $R = 0$ and $R = R_n$. The narrowness of the transition may complicate these tests, while special care must be taken to avoid TES self-heating, which can also mask the actual $R(T,J)$ dependences.

Hence, ideally the shape of the $R(T,J)$ should be explored through measurements avoiding self-heating, and with no elements which might disturb the current flow, such as metal features or absorber stems. We reported earlier two studies of the $R(T,I,H)$ transition in Mo/Au TESs (with sizes between 25×25 and $200 \times 200\,\mu m^2$), without membranes, absorber, and metal elements, and with high critical temperatures, $T_c \sim 467$–642 mK,[10,23] allowing the use of a ^{3}He refrigerator and thus minimizing the risk of TES heating. In those works, we showed that the lower half of the transition of those TES could be accounted for by a BKT (Berezinskii–Kosterlitz–Thouless)-like mechanism, i.e., depairing of vortex–antivortex pairs, enhanced by current. None of these TESs, however, showed any trace of WL effects because of their high T_c. We did observe the existence of WL effects in devices with the same design (also without membranes, absorbers, or normal metal features) and much lower T_c, ∼100 mK, at least up to TES lengths $L = 50\,\mu m$;[24] however, a dilution refrigerator—required for these low critical temperatures—enhances the risk of self-heating; even more, the resistance measurement setup in the dilution refrigerator did not allow for a detailed analysis of the lower part of the $R(T,J)$ transition in these devices. Therefore, from these two studies, on TES of different T_c and different sizes, it was not possible to clarify whether both transition mechanisms (BKT and WL) compete or one gives path to the other as the TES size changes. To our knowledge, among the many works devoted to analyze TES transition mechanisms, there are no other studies comparing the $R(T,J)$ shape of TESs with identical design and different sizes, which would allow addressing this issue.

In this paper, we analyze the position and shape of the superconducting transition as a function of size, bias current density, and temperature of Mo/Au TESs specially fabricated (design, size, and T_c) with this objective. We examine in detail the $R(T,J)$ shape of a batch of TESs of different sizes (width and length), with T_c specially tuned to work in a ^{3}He cryostat while still observing WL effects for the shorter devices. This allows observing how the BKT-like behavior in the lower half of the transition gives way to the RSJ behavior typical of devices with WL, as TES length and current decrease. Finally, we also analyze the upper part of the transition ($R > 70\%\ R_n$), where an enhanced conductivity is observed up to very high temperatures, due to the longitudinal proximity effect: for the shorter devices ($L \sim 8$–$10\,\mu m$), the resistance is still 95% R_n at temperatures three times higher than T_c and the effect is visible up to 8 times T_c. Our findings shed light on the interplay between TES size, driving current, and the dominant transition mechanism, providing insights useful for optimizing TES performance.

II. EXPERIMENTAL

Mo/Au TESs used in this study are constituted by a 70 nm-thick Mo film and a 195 nm-thick Au film, resulting in a bilayer critical temperature T_c of 373 mK. These thicknesses and T_c were carefully chosen because they allow working with a setup in a ^{3}He refrigerator, most suited for the intended measurements (see below), and still observe weak link effects for short enough TES lengths: indeed, the lower accessible temperature in a ^{3}He cryostat is typically 350 mK, while WL effects become weaker as the critical temperature of the TES increases.

TESs devoid of absorber, banks, and any other normal metal feature were fabricated on a bulk Si wafer covered with 0.5 mm-thick Si_3N_4; no membranes were open, in order to ensure a very good thermal contact between the device and the thermometer in the sample holder inside the cryostat. A single batch with TESs of different sizes was used for the purpose of this study; their detailed layout and fabrication procedures can be found elsewhere.[25] Basically, these TESs are rectangles of width w and length L; the latter corresponds to the distance between the Nb/Mo contacts, with a T_c of approximately 8.7 K. We will refer to the TESs by their size w × L without units, that is, TES 8×10 means a device with $w = 8\,\mu m$ and $L = 10\,\mu m$.

Because of the high Mo/Au bilayer T_c, in order to unambiguously observe WL effects, we had to decrease the explored range of TES lengths down to values close to $10\,\mu m$. The fabrication precision ensured by our photolithography process is below $1\,\mu m$. The nominal size vs the actual size was verified using optical microscopy or scanning electron microscopy (SEM). We, therefore, tested devices with sizes down to $8\,\mu m$.

07 January 2025 12:38:28

© Author(s) 2024

Measurements of resistance vs temperature $R(T)$ were conducted down to 350 mK employing a Physical Property Measurement System (PPMS) from Quantum Design equipped with a ^{3}He insert. Four-probe measurements, with current and voltage contacts placed on the Nb/Mo pads at each end of the TES and using a low-frequency (17 Hz) AC bias current, were carried out under nominal zero field cooling (ZFC) conditions. The system features a superconducting magnet with the demagnetizing option, ensuring a residual field below 0.5 Oe; however, experiments were carried out after cooling the magnet. The $R(T)$ runs were performed warming up in a controlled way, stabilizing each temperature. Bias currents were carefully chosen in order not to produce self-heating while allowing $R(T)$ measurements with enough sensitivity in the lower part of the transition for the purposed analyses and fits; the voltage resolution is <1 nV. The equipment's temperature control capability allowed for a minimum temperature step of $\Delta T = 1$ mK (temperature stability of 0.2%). This experimental setup and procedure, together with the bulk substrate (devices without membrane), ensured negligible self-heating; indeed, the measured transitions were verified to be reversible and reproducible, within the voltage and temperature sensitivities of the measurements.

The self-field was estimated to be at most ~1–2 μT, using $B_{self} \approx \mu_0 I/\pi L$;[26] this is one order of magnitude higher than the values obtained from the critical current $I_c(B)$ asymmetry in similar devices with $T_c \sim 100$ mK.[24] The effect of self-field on T_{c0} is expected to be negligible, since the shift of T_{c0} with magnetic field was determined as $dT_{c0}/dH \approx 0.05$ mK/μT for TESs with somehow higher critical temperature, $T_{c0} \sim 550$ mK.[10,23]

The residual square resistance of the bilayers is $R_{sq} = 33\ m\Omega \pm 2\ m\Omega$; it was determined from the R_n values of several TESs with length $L \geq 25\ \mu$m in order to avoid longitudinal proximity effects in shorter devices or small differences between the nominal and actual TES dimensions; details on the determination of R_n are given in Sec. III. The R_n values of the smaller TES (L,w = 8–10 μm) provide R_{sq} somehow higher, $R_{sq} = 46\ m\Omega \pm 3\ m\Omega$; the origin of this discrepancy is not clear. These R_{sq} values are consistent with values obtained for bilayers with other Mo and Au thicknesses, with different batches exhibiting small resistance changes.

III. RESULTS AND DISCUSSION

A. Position of the transition

The $R(T)$ transitions of several devices with different sizes were recorded at 10 μA; some of them are shown in Fig. 1, while Fig. 2 shows the extension of the $R(T)$ up to much higher temperatures. It can be observed that:

- Transitions are quite sharp, indicating good device quality.
- There is a significant *rounding* of the upper part of the transition (excess conductivity), extending to temperatures much higher than the onset of finite resistance (T_{c0}). This effect is not related to any fabrication defect: it is more pronounced for shorter TESs and low driving current densities. A similar behavior was observed in our devices with $T_c \sim 100$ mK (data not published) and has also been reported by Sadleir *et al.*[6,27] Due to this rounding, the normal state resistance (R_n) of each device was determined as the R value recorded at 7 K, where $R(T)$ can be considered flat, as expected for the residual resistance.
- There is a shift of the transition to higher temperatures as L is reduced, suggesting weak link (WL) effects, as described in Ref. 6. However, the critical temperatures T_{c0} recorded at 10 μA for TESs 16 × 60 and 8 × 8 differ only by 8 mK.

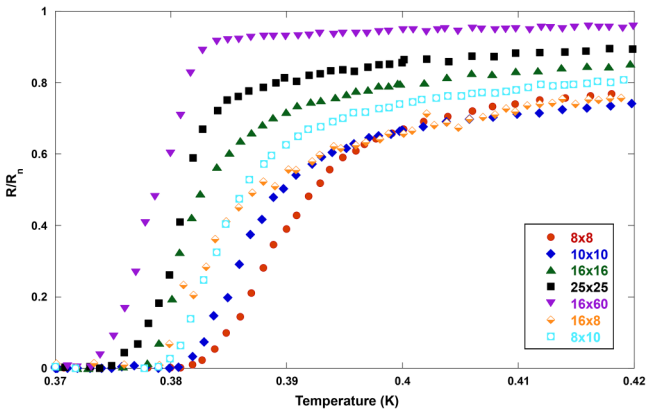

FIG. 1. Superconducting transition at 10 μA of TESs with different sizes (w × L).

Prior to analyzing T_{c0}(L), we must deal with the effects of the driving current density J. Figure 3 displays the evolution of the transition with J, for two TESs of significantly different lengths. For all devices, increasing the driving current shifts the transition to lower temperatures, as expected. Figure 4 displays T_{c0} as a function of the driving current density for several TESs with different sizes. The shift rate (dT_{c0}/dJ) is comparable to that observed in larger TESs with higher T_{c0}.[10] The data display a variety of slopes, which

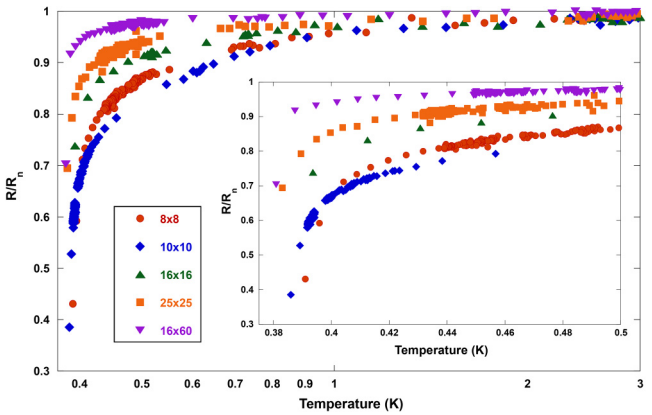

FIG. 2. $R(T)$ data for some TESs at 10 μA, recorded between 370 mK and 3 K. *Inset*: zoom of the region close to the superconducting transition. A significant rounding of the upper part of the transition, i.e., a smooth increase of resistance up to temperatures much higher than T_{c0}, is appreciated. This effect is enhanced as L decreases.

07 January 2025 12:38:28

© Author(s) 2024

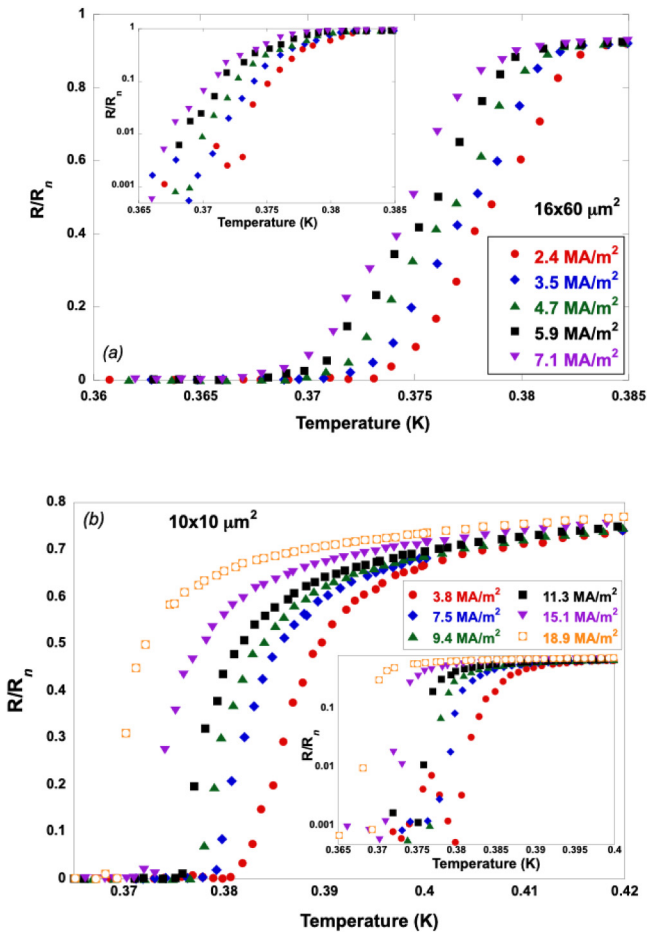

FIG. 3. R(T) data recorded at different driving currents for the 16 × 60 (a) and the 10 × 10 (b) TESs, respectively, representative of the behavior of long and short devices. *Insets*: same data in log Y-scale, which allows a better appraisal of the region close to zero resistance. For all TESs, the transition shifts to lower temperatures as the driving current is increased. For short TESs (b), the significant rounding of the upper part of the transition diminishes for increasing currents, resulting in a change of the transition shape in this region. For long TESs (a), with less relevant rounding, the transition shift looks rather parallel.

in part might be due to different $J_c(T=0)$ values for different devices, since T_c should depend on $J/J_c(T=0)$; however, this does not seem a plausible explanation for the different slopes of the 10 × 10 and 8 × 10 TESs.

Figure 5 shows the length dependence of the values of T_{c0} extrapolated or interpolated from the data in Fig. 4 at fixed low driving current densities; two different values were chosen in order to compare results because of the lack of saturation of $T_c(J)$ for the tested J window. The shorter devices (L = 8 and 10 μm) display unequivocally critical temperatures above those of the longer devices (L = 25 and 60 μm), which are equal within the temperature resolution. The T_c vs L^{-2} data can be roughly described as $\sim 1/L^2$. Therefore, there are visible weak link effects for the shorter TESs,

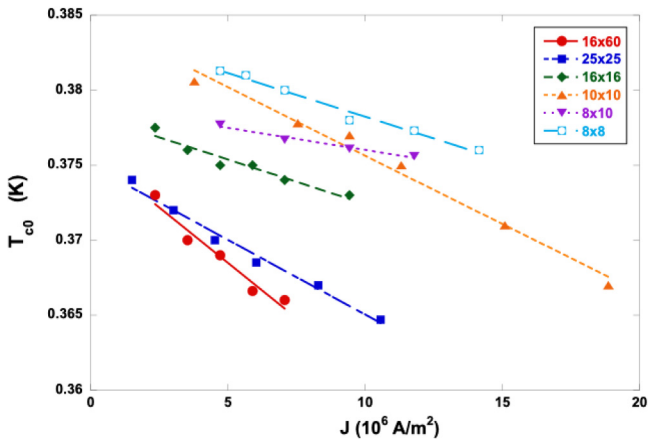

FIG. 4. Characteristic transition temperature T_{c0} (corresponding to the appearance of finite resistance) of selected devices, as a function of the driving current density.

albeit small (close to the resolution in temperature control, 1 mK). The WL effects are expected to diminish with longer lengths, as Fig. 5 reveals; we see below that this fact is supported by the inability to fit their $R(T)$ data with the WL model. The observed *weak* WL effects are due to both the high intrinsic critical temperature of the bilayers and the higher normal state resistance (thinner Au layer) as compared to 100 mK devices: both factors reduce the significance of WL effects.[6] From Fig. 5, we can determine an intrinsic critical temperature for the Mo/Au bilayer $T_{ci} = 373 \pm 1$ mK, in the low J limit explored in this work.

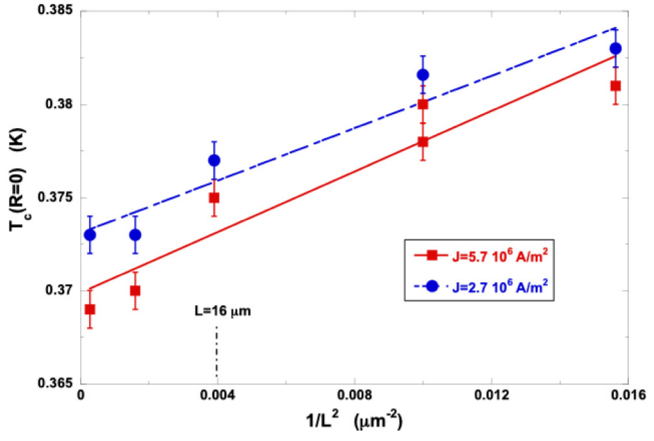

FIG. 5. Characteristic transition temperature T_{c0} at low driving current densities as a function of the inverse of the square of TES length. While TESs 25 × 25 and 16 × 60 display the same T_{c0} within the temperature resolution, TESs with L = 8 and 10 μm display higher T_{c0} values. The lines are fits to a T_{c0} vs $1/L^2$ dependence, pointing to the existence of WL effects at least for $L \lesssim 10\,\mu$m. The behavior of 16 × 16 TES is unclear, its T_{c0} lying very close to that of the longer devices.

07 January 2025 12:38:28

© Author(s) 2024

Figure 3 also reveals that the transition shape is dependent on L. The significant rounding of the upper part of the transition of the 10 × 10 TES is reduced for increasing currents, as already mentioned; this results in an apparent sharpening of the transition as J increases. The same behavior is observed for all small TESs (L = 8 and 10 μm), which evidence WL effects according to Fig. 5. The rounding effect is reduced, but present, in TES 16 × 16 and even in TES 25 × 25. For the 16 × 60 TES, the upper part of the transition remains nearly invariant, as reported for other large TESs.[10,23]

B. R(T,J) functional dependence

We proceed to analyze the functional dependence of $R(T,J)$ using two models. First, we consider the mechanism explored in Refs. 10 and 23, where it was demonstrated that the lower part of the transition (from $R = 0$ up to at least 45%–65% R_n) in larger ($L \sim 50$–$200\ \mu$m) devices with higher T_c (~450–650 mK) could be accounted for by a Berezinskii–Kosterlitz–Thouless (BKT)-like expression

$$\frac{R(T)}{R_n} = \mathrm{A}\ \exp\left(-b\left[\frac{T_c - T}{T - T'(I))}\right]^{1/2}\right). \tag{1}$$

The BKT transition[28] associates the onset of dissipation with the thermal depairing of magnetic vortex–antivortex pairs: once free, the vortices can move when a current is applied due to the Lorentz force, leading to a voltage drop (i.e., a finite resistance). A and b in Eq. (1) are constants: A < 1 and b is expected to be of the order of unity.[29] T_c is the mean field critical temperature of the device, and $T'(I)$ is the vortex–antivortex unbinding temperature; it should be close to T_{c0} but cannot be identified with it because T_{c0} is limited by the experimental resolution close to $R = 0$ and, therefore, expected to be somehow higher than $T'(I)$. It was suggested in Ref. 10 that the observed current dependence of T', not anticipated in the conventional BKT transition,[28] could be attributed to an enhancement of this effect by the current.

With the assumption that $T_c \gg T - T'(I)$, Eq. (1) can be approximated to

$$\ln\left(\frac{R(T)}{R_n}\right) = \mathrm{A} - \frac{b'}{\sqrt{T - T'(I)}}, \tag{1'}$$

which has the advantage of leaving only three fitting parameters, since T_c and b are absorbed into b'. Attempts were made to fit Eq. (1′) to all measured TESs and driving currents. The most satisfactory fits were obtained for TESs 25 × 25 and 16 × 60: for them, Eq. (1′) described the transition from $R = 0$ up to ~50% R_n, with a quality comparable to our previous works;[10,23] as an example, Fig. 6(a) displays the fits for TES 25 × 25, which provide $T'(I)$ values between 355 and 370 mK. The effectiveness of Eq. (1′) in describing the data diminishes as TES length is decreased [Fig. 6(b)] and is generally inadequate for L = 8 and 10 μm, with only occasional successes at higher currents. We consider the fits to be unsatisfactory when they either do not describe the data or partially describe it but providing unacceptable $T'(I)$ temperatures and/or inconsistent A′, b' values for different bias currents or TES sizes.

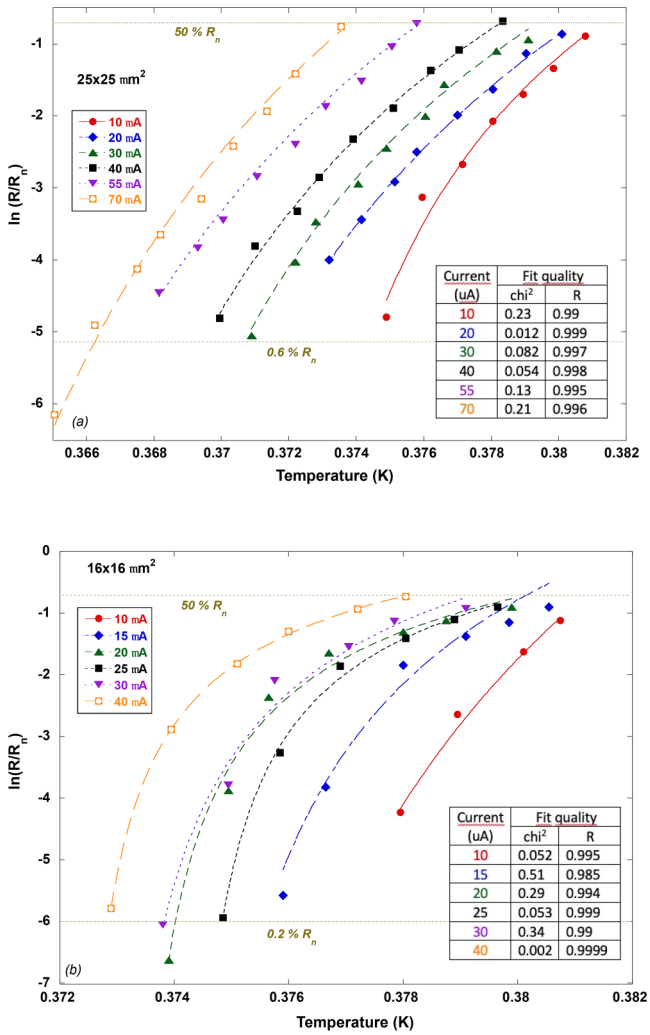

FIG. 6. Lower part of the transition of TESs 25 × 25 (a) and 16 × 16 (b). The lines are fits to Eq. (1′), corresponding to a BKT-like transition mechanism. Shown in the graphs are the parameters indicating the fits' quality, χ^2 and R. The fits are quite satisfactory for TES 25 × 25, representative of TES without visible WL effects; for the 16 × 16 TES, only the data recorded at the higher driving current looks satisfactory enough. See text for further details.

We conclude that the transition of TESs with significant WL effects is not well-captured by the BKT-like transition mechanism, while that of longer ($L \geq 25\ \mu$m) TESs is, consistent with prior findings.[10,23]

In fact, the resistively shunted junction (RSJ) model is expected to be applicable for devices exhibiting WL effects. In the low temperature limit, $R(T,J)$ in this model may be approximated to[5,26]

$$\frac{R(T)}{R_n} \cong \left[1 - \left(\frac{I_c(T)}{I}\right)^2\right]^{1/2}. \tag{2}$$

07 January 2025 12:38:28

© Author(s) 2024

Equation (2) requires knowing the functional dependence of $I_c(T)$ as an input, and this may greatly condition the resulting fits. We use the critical current of a TES displaying WL effects due to the longitudinal proximity effect induced by the pads,[6]

$$I_c(T) = \frac{F}{\xi^*}\, e^{-L/\xi^*}, \tag{3}$$

where F is expected to be nearly temperature independent and $\xi^*(T)$ is the effective coherence length. Close enough to the intrinsic critical temperature T_{ci} of the Mo/Au bilayer constituting the TES, $\xi^*(T)$ is given by[6,30]

$$\xi^* = \frac{\pi}{2}\xi_N \sqrt{\frac{T_{cL}}{T}} \frac{1}{|T/T_{ci} - 1|^{1/2}}. \tag{4}$$

Here, ξ_N is the normal state coherence length of the bilayer (i.e., above T_{ci}), and T_{cL} is the critical temperature of the leads. Note that ξ^* can be much larger than ξ_N when $T_{cL} \gg T_{ci}$ (a condition usually fulfilled by TESs).

Inserting in Eqs. (2) and (3) provides

$$\frac{R}{R_n} = \left[1 - C\,T\left|\frac{T}{T_{ci}} - 1\right| \exp\left(-D\sqrt{T\left|\frac{T}{T_{ci}} - 1\right|}\right)\right]^{1/2}, \tag{5}$$

where C and D are constants. Again, and in order to validate our conclusions, attempts were made to fit Eq. (5) to all TESs for all measured currents, using $T_{ci} = 373$ mK. This involved exploring different $\%R_n$ windows, and leaving C and D as fitting parameters. For L = 8 and 10 μm, Eq. (5) effectively describes the R(T) data at low currents up to resistance values close to 55% (Fig. 7), *but not higher up* in the transition. Attempts to fit the data for higher currents for these devices were unsuccessful or yielded unacceptable parameters (these are the data sets without displayed fits in Fig. 7). Similarly, meaningful fits could not be obtained for TESs with L $\geq$ 16 μm.

Therefore, the analyses conducted so far are consistent and provide the following insights:

- The RSJ model, incorporating the effective coherence length enhanced by the longitudinal proximity effect, can accurately describe the lower part of the transition in TESs exhibiting WL effects at sufficiently low currents.
- As the WL effect diminishes or disappears due to an increase in the driving current density J or in the TES length L, the RSJ model becomes inadequate. Instead, a BKT-like mechanism can explain the lower part of the transition in TESs without WL effects.
- The extent of the WL-dominated regime primarily depends on the longitudinal proximity effect, which, in turn, is governed by the effective coherence length $\xi^*(T)$. According to Eq. (4), larger ξ_N (i.e., lower square resistances of the proximity bilayer constituting the TESs) or higher T_{cL}/T_{ci} ratios enhance $\xi^*(T)$, leading to an increase in the critical current of the TES. Consequently, this enhances the maximum TES length and the maximum driving current $J \sim$ I/w that allow the observation of WL effects. For instance, WL effects are visible in the Mo/Au devices explored in this work (with $T_{ci} = 373$ mK) for L $\leq$ 10 μm, while the behavior of the 16 × 16 device is unclear. However, TESs with $T_{ci} = 100$ mK exhibit unambiguous WL effects up to significantly longer lengths.[3,6,24] This fact is attributed to both higher T_{cL}/T_{ci} ratios and lower resistances of the bilayers, constituted by thicker Au layers. Another factor to be taken into account, regarding the driving current effect on the observed dominant transition mechanism, is that high J values, in addition to diminishing WL effects, are expected to promote vortex depairing in the case of the BKT-like mechanism, as argued in Ref. 10.
- Neither the RSJ model—at least its approximation given by Eq. (2)—nor the BKT-like transition mechanism is capable of describing the upper part of the resistive transition (above ~60% R_n). This region is characterized by significant rounding of the $R(T)$ close to the onset of the resistance drop, especially pronounced as L and J decrease (Figs. 1 and 2).

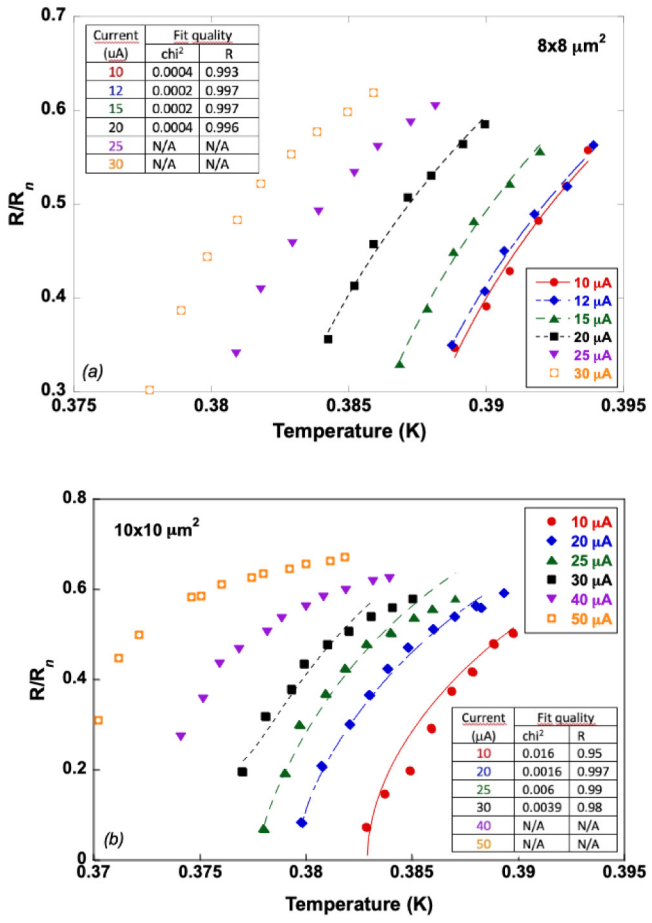

FIG. 7. Lower part of the transition for TESs 8 × 8 (a) and 10 × 10 (b), both displaying evidence of WL effects (see Fig. 5). The lines are fits to Eq. (5), corresponding to the RSJ model. Data at the higher currents could not be fitted with reasonable fitting parameters. Shown in the graphs are the parameters indicating the fits' quality, χ^2 and R.

07 January 2025 12:38:28

© Author(s) 2024

Hence, attention is now driven toward the upper part of the transition, closer to R_n. Traditionally, a rounding of the upper part of the superconducting transition is due to thermal fluctuations, resulting in excess conductivity (paraconductivity) near T_c. We have considered the Aslamazov–Larkin paraconductivity in a 2D superconductor[31] and also the paraconductivity in a Josephson junction.[32] Neither can accurately reproduce the experimental data: the significant rounding above 60% R_n results in very narrow fitting windows and/or implausible, too low T_c values.

However, the rounding can be impressively described by assuming a reduction of the residual (normal state) resistance above T_c as T decreases, owing to the significant enhancement of the effective coherence length due to the longitudinal proximity effect induced by the pads [see Eq. (4) and discussion above]. Considering that the TES regions within a length ξ* close to the pads remain superconducting above the TES transition and, therefore, do not contribute to R_n, we can roughly express the measured resistance by the following rescaling:

$$R \approx \frac{R_n}{L}\,(L - 2\xi^*), \tag{6}$$

where the effective coherence length $\xi^*(T)$ is given by Eq. (4). Substituting it, we obtain

$$\frac{R}{R_n} \approx \left(1 - \frac{2\xi^*}{L}\right) = \left(1 - \frac{B}{\sqrt{T}\sqrt{|T/T_{ci} - 1|}}\right), \tag{7}$$

with $B \equiv \frac{\pi}{L}\xi_N\sqrt{T_{cL}}$.

Examples of the fits to Eq. (7) are depicted in Fig. 8. These fits were achieved by setting $T_{ci} = 373$ mK and employing two fitting parameters: B and a proportionality factor that consistently yields values very close to unity. The fits are quite satisfactory and encompass the data from around ~70%R_n up to temperatures significantly higher than T_{c0}, as illustrated in the inset of Fig. 8(a).

To our knowledge, only Sadleir *et al.*[6,27] have reported data of enhanced conductivity in the region R/R_n above ~50% and its dependences on magnetic field and current, in Mo/Au TESs with $T_c \sim 100$ mK. In Ref. 27, this effect is also attributed to the longitudinal proximity effect, with the regions close to the contacts becoming superconducting and not contributing to the normal state resistance; however, aside from the lower T_c of the devices, Ref. 27 has two differences with the data and analysis reported here: (i) we analyze a wider temperature window above T_c (up to nearly 8 times higher) and (ii) the authors use the normal state coherence length ξ_N as the characteristic length of the extent of the superconducting regions near the contacts. The magnitude and expression of the relevant coherence length in TESs with longitudinal proximity effect was discussed in Ref. 30, where it was concluded that the effective coherence length of the bilayer is

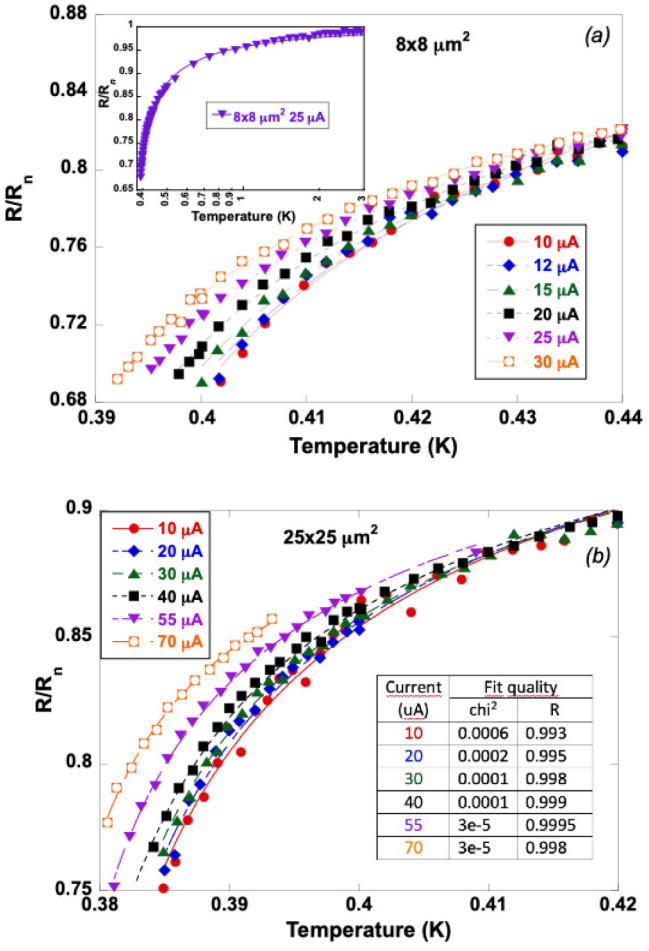

FIG. 8. Upper part of the transition for TESs 8 × 8 (a) and 25 × 25 (b). The lines are fits to Eq. (7). *Inset* in (a): Fit of the upper part of the transition to Eq. (7) up to 3 K, for TES 8 × 8. (b) displays also the parameters indicating the fits' quality, χ^2 and R.

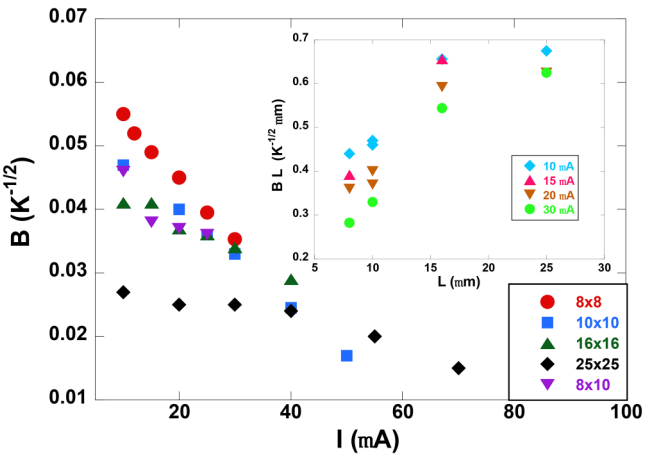

FIG. 9. B parameter obtained from the fits to Eq. (7) of the upper part of the R(T) transition recorded at different currents in TESs with variable sizes. Inset: dependence of B × L on L, at different driving currents.

07 January 2025 12:38:28

© Author(s) 2024

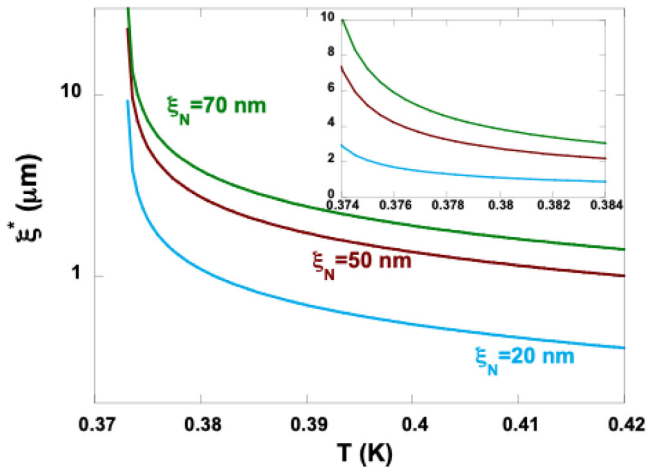

FIG. 10. Calculated TES effective coherence length ξ* using Eq. (4), for three values of ξ_N, using T_{ci} = 373 mK. *Inset:* zoom close to T_{ci}.

enhanced by the higher T_c of the leads, as given by Eq. (4) and used in Eq. (7).

The fitting parameter B is expected to be current independent and vary as 1/L. It is depicted in Fig. 9. While a decrease of B with L is evident, the dependence is less steep than 1/L, resulting in an apparent increase of $B\,x\,L \propto \xi^*$. Additionally, the dependences of B on L and on driving current tend to become smoother with increasing driving currents and L, that is, when the WL effects are weakened.

The obtained values of B yield ξ_N values ranging between 18 and 72 nm, which correspond to ξ* values of ∼μm. These values align with the observed WL effect in our smaller devices. To illustrate this, ξ*(*T*) was calculated using Eq. (4) and three different values for ξ_N. The results are depicted in Fig. 10. For $\xi_N = 50$ nm, a value close to the average obtained from our fits, we obtain $\xi^* = 8\,\mu$m at $T = 375$ mK, and $\xi^* = 4\,\mu$m at $T = 378$ mK, consistent with the observed magnitude of the shift of T_c with L (Fig. 1).

Therefore, the effective reduction of R_n because of the longitudinal proximity effect appears as a plausible explanation for the observed rounding of the upper part of the transition. However, the effect of current remains to be elucidated. The general expression of the RSJ model[5] might offer some insight.

IV. CONCLUSIONS

In this study, we conducted a comprehensive analysis of the transition shape *R*(*T*,*I*) of bare Mo/Au TES with bilayer critical temperature $T_{ci} = 373$ mK, investigating its dependence on current and device size. Our findings can be summarized as follows:

- Short enough TESs display weak link (WL) effects, demonstrating their persistence even at temperatures close to 400 mK albeit diminishing as T_c increases, as expected. For these devices, the RSJ model, incorporating a critical current $I_c(T)$ determined by the effective coherence length enhanced by the longitudinal proximity effect of the pads, ξ*, adequately describes the *R*(*T*,*I*) behavior of the lower half of the transition (roughly up to 50% R_n).
- With increasing TES length or driving current density, the WL effects tend to vanish. Then, a flux motion mechanism associated with the depairing of vortex–antivortex pairs (similar to the Berezinskii–Kosterlitz–Thouless transition, but enhanced by current) becomes a plausible explanation for the lower half of the transition (again from $R = 0$ up to roughly 50% R_n).
- A rounding of the upper part of the *R*(*T*) transition was observed, becoming more prominent as the TES length decreases: it results in a resistance significantly lower than the normal state resistance up to temperatures quite above T_c (up to eight times). For R > 70% R_n, this effect is accounted for by considering that the normal state resistance R_n of the devices is effectively reduced by a factor $1 - 2\xi^*/L$. This rescaling of R_n roughly corresponds to the regions of length ξ* close to the pads becoming superconducting because of the longitudinal proximity effect induced by them and, therefore, not contributing to R_n. Nonetheless, there are remaining details to be explained, such as the current dependence of the extracted ξ* or the decrease of *R* at very high temperatures, $T \gg T_{c0}$ (above 90% R_n). These effects could be addressed by a more refined model than the one tentatively tested here.

This study underscores the significance of the TES transition mechanisms in determining TES performances, particularly the logarithmic derivatives, with implications for TES stability, noise, and energy resolution. Furthermore, it highlights the importance of a careful analysis when examining the behavior of TESs with varying w and L. Last, the substantial rounding of the upper part of the transition or, in other words, the effective decrease of the normal state resistance, observed up to temperatures much higher than the T_{c0} of the devices, suggests that extracting R_n from I–V curves might be challenging, and might introduce small errors that could propagate to the TES parameters extracted from dark characterization; we note also that this rounding can cover a significant part of the *R*(*T*) transition for short enough TES (down to $R/R_n \sim 50\%$–60% for devices with $T_c \sim 100$ mK), thus giving the appearance of quite broad transitions, reducing α, and masking the actual superconducting transition.

07 January 2025 12:38:28

ACKNOWLEDGMENTS

This work has been carried out with financial support from the European Union's Horizon 2020 Research and Innovation Programme under Grant Agreement No. 871158 (Project AHEAD2020) and from the Spanish Ministerio de Ciencia e Innovación MICINN (Project PID2021-122955OB-C42). L.F. acknowledges also Spanish MICINN for support through the Severo Ochoa Programme for Centres of Excellence (Project FUNFUTURE, CEX2019-000917-S).

AUTHOR DECLARATIONS

Conflict of Interest

The authors have no conflicts to disclose.

© Author(s) 2024

Author Contributions

Lourdes Fàbrega: Conceptualization (lead); Formal analysis (lead); Methodology (lead); Writing – original draft (lead); Writing – review & editing (lead). **Agustín Camón:** Investigation (supporting); Resources (equal); Writing – review & editing (supporting). **Carlos Pobes:** Investigation (supporting); Resources (supporting); Writing – review & editing (supporting). **Pavel Strichovanec:** Investigation (supporting); Resources (supporting).

DATA AVAILABILITY

The data that support these findings are available from the corresponding author upon reasonable request.

REFERENCES

[1]K. D. Irwin and C. C. Hilton, in *Topics in Applied Physics*, edited by C. Enss (Springer-Verlag, Berlin, 2005), Vol. 99, pp. 63–150.
[2]L. Gottardi and K. Nagayashi, Appl. Sci. **11**, 3793 (2021).
[3]L. Gottardi *et al.*, Phys. Rev. Lett. **126**, 217001 (2021).
[4]M. Galeazzi, IEEE Trans. Appl. Supercond. **21**, 267 (2011).
[5]A. Kozorezov *et al.*, Appl. Phys. Lett. **99**, 063503 (2011).
[6]J. E. Sadleir *et al.*, Phys. Rev. Lett. **104**, 047003 (2010).
[7]D. A. Bennett *et al.*, J. Low Temp. Phys. **167**, 102 (2012).
[8]D. A. Bennett *et al.*, Appl. Phys. Lett. **104**, 042602 (2014).
[9]G. W. Fraser, Nucl. Instrum. Methods Phys. Res. A **523**, 234 (2004).
[10]L. Fàbrega *et al.*, Supercond. Sci. Technol. **32**, 015006 (2019).
[11]S. Ezaki *et al.*, J. Appl. Phys. **123**, 084504 (2018).
[12]L. Gottardi *et al.*, Appl. Phys. Lett. **105**, 162605 (2014).
[13]M. Kounalakis *et al.*, Phys. Rev. Appl. **20**, 024017 (2023).
[14]M. A. Lindeman *et al.*, Rev. Sci. Instrum. **75**, 1283 (2004).
[15]S. J. Smith *et al.*, J. Appl. Phys. **114**, 074513 (2013).
[16]N. A. Wakeham *et al.*, J. Low Temp. Phys. **193**, 231 (2018).
[17]K. M. Morgan *et al.*, Appl. Phys. Lett. **110**, 212602 (2017).
[18]Y. Zhou *et al.*, J. Low Temp. Phys. **193**, 321 (2018).
[19]S. Zhang *et al.*, J. Appl. Phys. **121**, 074503 (2017).
[20]Y. Zhou, J. Phys.: Conf. Ser. **1590**, 012032 (2020).
[21]M. de Wit *et al.*, J. Appl. Phys. **128**, 223902 (2020).
[22]N. A. Wakeham *et al.*, J. Appl. Phys. **125**, 164503 (2019).
[23]L. Fàbrega *et al.*, communication to LTD18 (2019), see https://agenda.infn.it/event/15448/contributions/95536/attachments/65508/79783/117_fabrega_poster.pdf or https://digital.csic.es/handle/10261/208827.
[24]L. Fàbrega *et al.*, J. Low Temp. Phys. **209**, 287–292 (2022).
[25]C. Pobes *et al.*, IEEE Trans. Appl. Supercond. **27**, 2101505 (2017).
[26]J. E. Sadleir, Ph.D. thesis (University of Illinois at Urbana-Champaign, 2010).
[27]J. E. Sadleir *et al.*, Phys. Rev. B **84**, 184502 (2011).
[28]B. I. Halperin and D. R. Nelson, J. Low Temp. Phys. **36**, 599 (1979).
[29]A. M. Kadin, K. Epstein, and A. M. Goldman, Phys. Rev. B **27**, 6691 (1983).
[30]J. N. Ullom and D. A. Bennett, Supercond. Sci. Technol. **28**, 084003 (2015).
[31]L. G. Aslamazov and A. I. Larkin, Sov. Phys. Solid State **10**, 875 (1968).
[32]R. A. Ferrell, J. Low Temp. Phys. **1**, 423 (1969).

07 January 2025 12:38:28

© Author(s) 2024